Substrate Specificity of OXA-48 after $\beta5-\beta6$ Loop Replacement

Laura Dabos, Agustin Zavala, Rémy Bonnin, Oliver Beckstein, Pascal Retailleau, Bogdan Iorga, Thierry Naas

▶ **To cite this version:**

Laura Dabos, Agustin Zavala, Rémy Bonnin, Oliver Beckstein, Pascal Retailleau, et al.. Substrate Specificity of OXA-48 after $\beta5-\beta6$ Loop Replacement. ACS Infectious Diseases, 2020, 6 (5), pp.1032-1043. ⟨10.1021/acsinfecdis.9b00452⟩. ⟨hal-02841835⟩

HAL Id: hal-02841835

https://hal.science/hal-02841835v1

Submitted on 7 Dec 2020

HAL is a multi-disciplinary open access archive for the deposit and dissemination of scientific research documents, whether they are published or not. The documents may come from teaching and research institutions in France or abroad, or from public or private research centers.

L'archive ouverte pluridisciplinaire **HAL**, est destinée au dépôt et à la diffusion de documents scientifiques de niveau recherche, publiés ou non, émanant des établissements d'enseignement et de recherche français ou étrangers, des laboratoires publics ou privés.

HAL Authorization

Substrate specificity of OXA-48 after β5-β6 loop replacement.

Laura Dabos[‡§#], Agustin Zavala[‖#], Rémy A. Bonnin[‡§⊥], Oliver Beckstein[†], Pascal Retailleau[‖], Bogdan I. Iorga[‖*], Thierry Naas[‡§⊥⊤*]

‡ EA7361 "Structure, dynamic, function and expression of broad spectrum β-lactamases", Université Paris Sud, Université Paris Saclay, LabEx Lermit, Faculty of Medicine, 94270 Le Kremlin-Bicêtre, France.

§ Evolution and Ecology of Resistance to Antibiotics Unit, Institut Pasteur – APHP -Université Paris Sud, 75015 Paris, France

‖ Institut de Chimie des Substances Naturelles, CNRS UPR 2301, Université Paris-Saclay, Labex LERMIT, 91190 Gif-sur-Yvette, France.

⊥ Associated French National Reference Center for Antibiotic Resistance: Carbapenemase-producing Enterobacteriaceae, 94270 Le Kremlin-Bicêtre, France.

† Department of Physics and Center for Biological Physics, Arizona State University, Tempe, 85281 Arizona, USA.

⊤ Bacteriology-Hygiene unit, Assistance Publique/Hôpitaux de Paris, Bicêtre Hospital, 94270 Le Kremlin-Bicêtre, France.

OXA-48 carbapenemase has rapidly spread in many countries worldwide with several OXA-48-variants being described, differing by a few amino acid (AA) substitutions or deletions, mostly in the β5-β6 loop. While single AA substitutions have only minor impact on OXA-48 hydrolytic profiles, others with 4 AA deletions result in loss of carbapenem hydrolysis and gain of expanded-spectrum cephalosporin (ESC) hydrolysis. We have replaced the β5-β6 loop of OXA-48 with that of OXA-18, a clavulanic-acid inhibited oxacillinase capable of hydrolyzing ESCs but not carbapenems. The hybrid enzyme OXA-48Loop18 was able to hydrolyze ESCs and carbapenems (although with a lower k_{cat}), even though the β5-β6 loop was longer and its sequence quite different from that of OXA-48. The kinetic parameters of OXA-48Loop18 were in agreement with the MIC values. X-ray crystallography and molecular modeling suggest that the conformation of the grafted loop allows the binding of bulkier substrates, unlike that of the native loop, expanding the hydrolytic profile. This seems to be due not only to differences in AA sequence, but also to the backbone conformation the loop can adopt. Finally, our results provide further experimental evidence for the role of the β5-β6 loop in substrate selectivity of OXA-48-like enzymes and additional details on the structure-function relationship of β-lactamases, demonstrating how localized changes in these proteins can alter or expand their function, highlighting their plasticity.

Carbapenemase, expanded-spectrum cephalosporins, β5-β6 loop, oxacillinases.

Ambler class D β-lactamases (DBLs), also known as oxacillinases, are active site serine β-lactamases like the Ambler classes A and C [1,2]. DBLs form a very heterogeneous family of enzymes, differing both at genetic and biochemical levels, with enzymes possessing low sequence identities and various substrate profiles going from narrow- to extended-spectrum of hydrolysis, sometimes including carbapenems [3]. The Carbapenem-Hydrolyzing class D β-Lactamases (CHDLs) may be divided in three groups: i) OXA-48 from *Enterobacteriaceae*; ii) OXA-23/-40/-58/-143 reported mostly from *Acinetobacter baumannii* and iii) OXA-198 from *P. aeruginosa* [4]. None of these enzymes possess the ability to hydrolyze significantly both expanded-spectrum cephalosporins (ESCs) and carbapenems and the hydrolysis of carbapenems by CHDLs remains low, due to their poor catalytic efficiency towards those β-lactam molecules [5].

β-Lactamases of OXA-48-type are the most worrisome, given their rapid spread in many countries worldwide and their propensity to evolve by mutations leading to various phenotypic expressions [6]. Although OXA-48 hydrolyzes penicillins at a high level and carbapenems at a low level, it shows (almost) no activity against ESCs [7]. OXA-48 producers, initially described in *K. pneumoniae* isolates from Turkey in 2004, have since been extensively reported from all continents [8–10]. OXA-48 represents 85% of the carbapenemases isolated in France [11] and numerous outbreaks have been described with associated high mortality rates [12]. Since the first identification of OXA-48, different variants have been reported, differing by few amino acid substitutions or deletions. For a complete list of variants see the Beta-Lactamase DataBase [2] (http://bldb.eu/BLDB.php?class=D#OXA) and the "Bacterial Antimicrobial Resistance Reference Gene Database" (https://www.ncbi.nlm.nih.gov/pathogens/isolates#/refgene/). In addition, a large-scale analysis of genomic data revealed an additional unexpected variety of OXA-48-like enzymes [13]. Whereas some OXA-48-variants with single amino acid substitutions have similar hydrolytic activities as OXA-48, others, such as OXA-163 [14,15], OXA-247[16], or OXA-405[17,18], have a four amino acid (AA) deletion that results in the loss of carbapenem- hydro

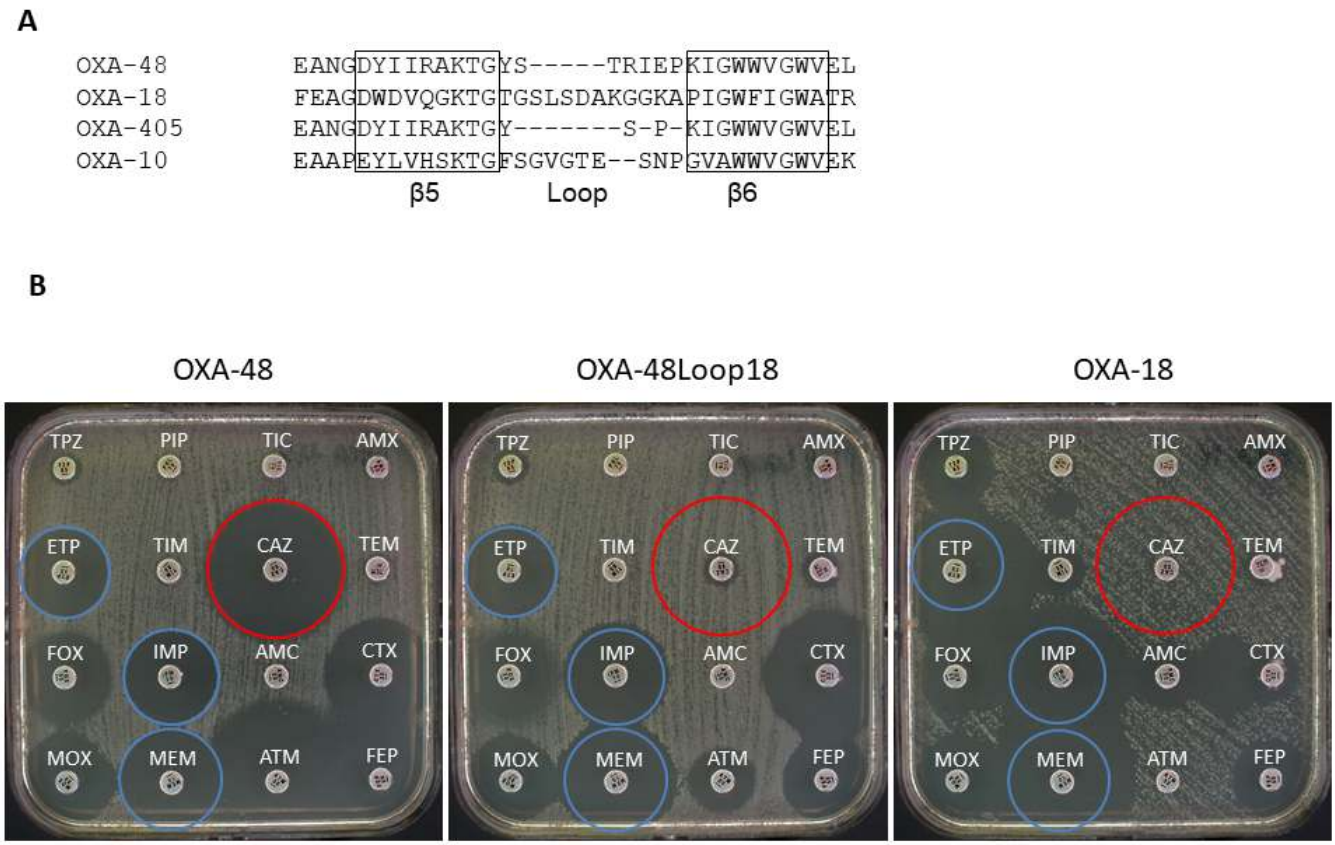

Figure 1. A) Sequence alignment of the β5-β6 loops of OXA-48, OXA-18, OXA-405 and OXA-10. B) Antibiograms of E. coli TOP10 harboring plasmids pTOPO-OXA-48, pTOPO-OXA-48Loop18, and pTOPO-OXA-18. TPZ: Piperacillin-tazobactam, PRL: Piperacillin, TIC: Ticarcillin, AML: amoxicillin, ETP: Ertapenem, TIM: Ticarcillin-clavulanic acid, CAZ: Ceftazidime, TEM: Temocillin, FOX: Cefoxitin, IPM: Imipenem, AMC: Amoxicillin-clavulanic acid, CTX: Cefotaxime, MOX: Latamoxef, MEM: Meropenem, ATM: Aztreonam, FEP: Cefepime. Blue circles show carbapenem inhibition zones of OXA-48, red circles show ceftazidime inhibition zones of OXA-48.

lysis and gain of ESC hydrolysis [7,14,16,17]. They actually exhibit a substrate profile that is similar to that of OXA-18, an OXA-Extended-Spectrum β-lactamase (OXA-ESBL) identified in *P. aeruginosa*, with the difference that they are not susceptible to clavulanic acid inhibition[19].

Until now, more than 175 crystal structures of different class D sub-families have been deposited in PDB database [2]. Despite a remarkable sequence divergence between these oxacillinases, their overall fold is similar and the active site elements are well conserved [20]. Previously, it was described that the orientation and size of the β5-β6 loop of OXA-48 is different from that of OXA-10, a class D β-lactamase with no activity against carbapenems, suggesting a major role of this loop in carbapenem hydrolysis [20,21]. The replacement of the β5-β6 loop in OXA-10 by that of OXA-48 turned the chimeric enzyme into a carbapenemase [20,21]. This loop is close to the active site and connects two β-strands which delimit one side of the active site in OXA-48, one of them including the catalytically-relevant conserved KTG residues [20]. Alignment of the β5-β6 loop of OXA-48 with that of OXA-10, OXA-405 and OXA-18 is shown on Fig. 1A. Not only the length and the sequence of the loops are different, but also the hydrolysis profiles of these enzymes. Reducing the length of the loop of OXA-48 by 4 AAs results in an enzyme that lost carbapenem hydrolysis, but gained ESC, as well as aztreonam, hydrolytic activity [17,18]. OXA-10 has a longer loop and displays a broad-spectrum profile with no significant carbapenem and low-level ESC hydrolysis. The loop of OXA-18 is even longer, and this enzyme displays high level of ESC and aztreonam hydrolysis, and shows a strong clavulanic acid inhibition, which is unusual for oxacillinases [3].

To further analyze the role of the β5-β6 loop of OXA-48 carbapenemase in respect to the carbapenem-hydrolysis, as well as ESC hydrolysis, we substituted the β5-β6 loop of OXA-48 with that of the OXA-ESBL, OXA-18. We evaluated the hydrolysis profile of this OXA-48Loop18 hybrid enzyme and determined its crystallographic structure that constituted the starting point for covalent docking and molecular dynamics simulations, in order to explain the observed profile.

Results

Alteration in the susceptibility profile of OXA-48

The antimicrobial susceptibility profiles, determined by disk diffusion (Fig. 1B) and minimal inhibitory concentrations

(MICs) for several β-lactams, conferred by OXA-48, OXA-18 and the hybrid OXA-48Loop18, was obtained by cloning the corresponding genes in pCR-Blunt II-Topo kit (Invitrogen) and expressing them into *E. coli* TOP10 (Table 1). The three proteins conferred resistance to penicillins. OXA-18 conferred, as previously described [19], a typical ESBL profile e.g. resistance to ESCs and a synergy image between ESC and clavulanic acid on a disk diffusion antibiogram. *E. coli* Top10 (pTOPO-OXA-18) presented very low MIC values for carbapenems. On the other hand, OXA-48 conferred a reduced susceptibility to carbapenems and very low MIC values for ESCs [8].

Table 1. MICs of β-lactams for *E. coli* TOP10 pTOPO-OXA-48, *E. coli* TOP10 pTOPO-OXA-48Loop18, *E. coli* TOP10 pTOPO-OXA-18 and *E. coli* TOP10.

Antibiotic	MIC (mg/L)			
	E. coli TOP10			*E. coli* TOP10
	(pTOPO-OXA-48)	(pTOPO-OXA-48Loop18)	(pTOPO-OXA-18)	
Amoxicillin	>256	>256	>256	2
Amoxicillin + CLA[a]	>256	32	8	2
Piperacillin	>256	>256	>256	1.5
Cefotaxime	0.75	0.19	>32	0.06
Ceftazidime	0.19	48	>256	0.12
Cefepime	0.19	2	12	0.023
Imipenem	0.75	0.38	0.25	0.25
Meropenem	0.25	0.094	0.047	0.016
Ertapenem	0.25	0.25	0.094	0.003
Temocillin	>1024	64	96	4
Aztreonam	0.047	8	>256	0.047

[a]CLA, clavulanic acid (2mg/L).

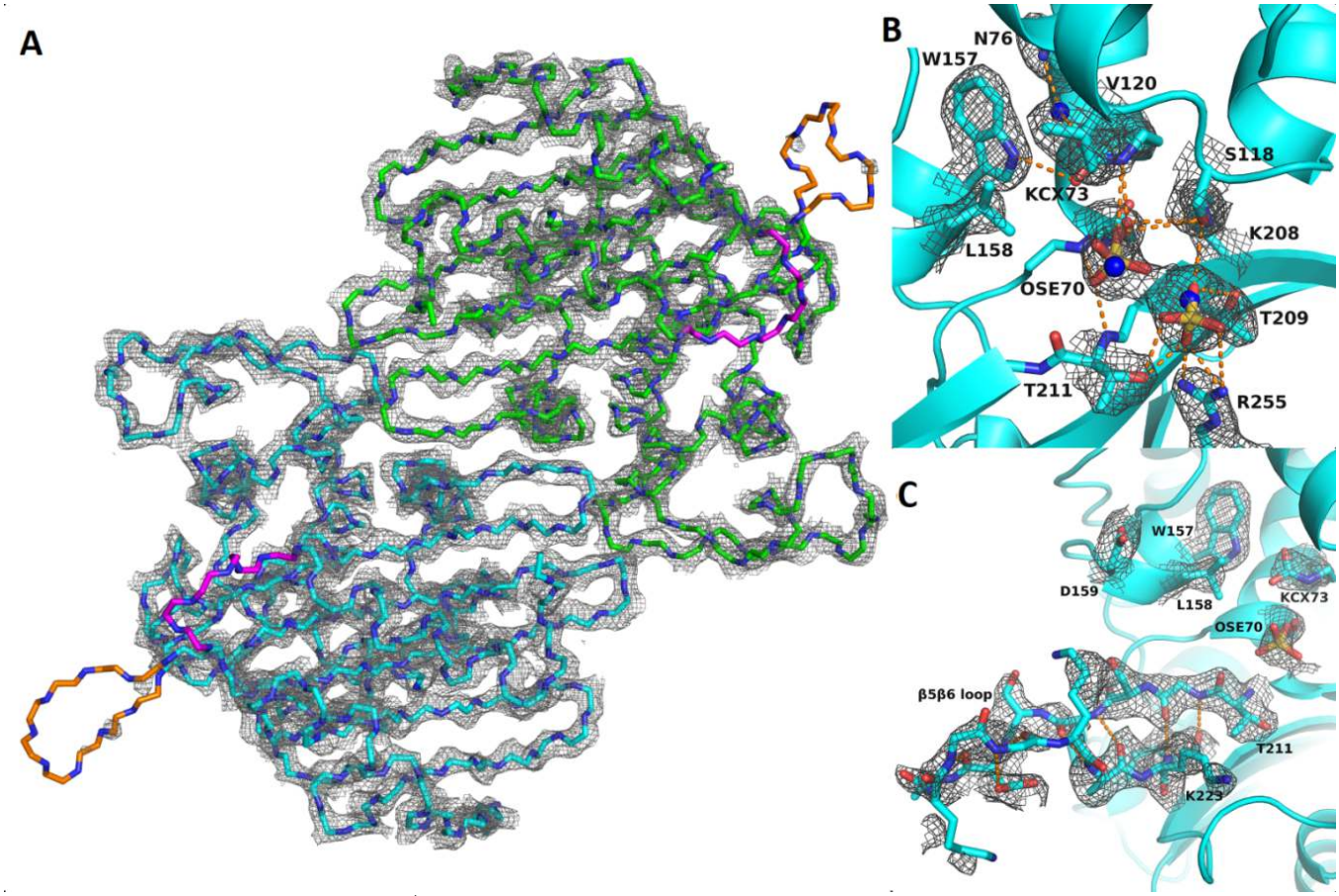

Figure 2. Crystal structure of OXA-48loop18. A) Overview of crystal structure. For clarity, only the backbone atoms and their electron density is shown, depicted at 2.0 σ. Chains A and B are colored green and cyan, respectively. β5-β6 and β7-α10 loops, which are depicted in orange and magenta, respectively, are more flexible than the rest of the protein, as evidenced by their weaker electron density. B) Active site cavity of chain B. Backbone represented as cyan ribbon, relevant residues are shown as cyan sticks, hydrogen bonds as orange dashed lines, and sulfate anions as yellow and red sticks. OSE: O-sulfo-serine. KCX:

carbamylated lysine. Electron density is represented at 1.0 σ, so as to evidence electron density around partially occupied OSE, sulfate, and waters (see results). Water molecules are represented as blue spheres to evidence their superposition with the sulfate molecules. C) β5-β6 loop of chain B. Electron density is represented at 1.0 σ for the β5-β6 loop, showing weaker but clear electron density that allows for the backbone as well as for most sidechains to be modelled. Hydrogen bonds show the further extension of the β5 and β6 strands.

Table 2. Steady-state kinetic parameters of β-lactamases OXA-48, OXA-48Loop18 and OXA-18.

Substrate	K_m(μM)			k_{cat} (s^{-1})			k_{cat}/K_m ($mM^{-1} s^{-1}$)		
	OXA-48[a]	OXA-48Loop18	OXA-18	OXA-48[a]	OXA-48Loop18	OXA-18	OXA-48[a]	OXA-48Loop18	OXA-18
Ampicillin	395	43	8	955	4	2.1	2418	92	259
Cefalotin	195	124	42	44	0.5	34	226	4.3	804
Cefoxitin	>200	77	9	>0.05	0.004	0.302	0.3	0.05	35
Ceftazidime	N.H	>1000	44	N.H	>0.2	10	N.H	0.2	236
Cefotaxime	>900	>1000	54	>9	>3.1	62	10	2.4	1158
Cefepime	>550	357	78	>0.60	0.4	19	1.1	1.1	248
Imipenem	13	109	13	5	0.4	0.006	369	3.2	0.5
Meropenem	11	16	71	0.07	0.01	0.01	6	0.7	0.2
Ertapenem	100	15	12	0.13	0.02	0.01	1.3	1.1	0.9
Aztreonam	N.H	>1000	14	N.H	>1.3	3.3	N.H	0.7	234

Errors for determined kinetic values were below 10%. NH, Hydrolysis could not be detected with concentrations of substrate and enzymes up to 1000 μM and 400 nM, respectively.

[a] values were from Docquier *et al*[20]

Interestingly, *E. coli* Top10 (pTOPO-OXA-48Loop18) presented a susceptibility profile that seems to be a combination of both. It was resistant to penicillins, ceftazidime and presented a reduced susceptibility to cefepime (MIC 2 mg/L). Additionally, a synergy with clavulanic acid was also observed but not as marked as with *E. coli* Top10 (p- TOPO-OXA-18). At the same time, it showed lower MIC values for carbapenems as compared to those of *E. coli* Top10 (pTOPO-OXA-48) but higher than those of *E. coli* Top10 (pTOPO-OXA-18). In a similar manner, MIC values for aztreonam ranged between the two native enzymes, while for temocillin the hybrid mutant presented the lowest value.

Kinetic analysis

To evaluate the biochemical properties, steady-state kinetic parameters were determined to compare the catalytic efficiencies of OXA-48 with that of OXA-18 and OXA-48Loop18 (Table 2). The catalytic efficiency for ampicillin was highest for OXA-48, followed by that of OXA-18 and OXA-48Loop18. In the last two cases, the reduced catalytic efficiencies were due to lower k_{cat} values, even though the K_ms were at least 10-fold lower. Unlike OXA-48, OXA-48Loop18 was able to hydrolyze ceftazidime, but with lower catalytic efficiency than OXA-18. These kinetic data were in agreement with the observed MIC values. For imipenem, the highest catalytic efficiency was observed with OXA-48, whereas that of OXA-48Loop18 was 100-fold lower, as a result of a 10-fold higher K_m and a 10-fold lower k_{cat}. Interestingly with meropenem, and even more with ertapenem, these hydrolytic differences between OXA-48 and OXA-48Loop18 were less important. For ertapenem, similar values were found as a consequence of 10-fold lower K_m for OXA-48Loop18, even though the k_{cat} was 6-fold lower. These small differences were enough to increase the MIC values of *E. coli* expressing OXA-48Loop18 from 0.094 mg/L (conferred by OXA-18) to 0.25 mg/L, a value comparable to that conferred by OXA-48.

Thermostability analysis

In order to evaluate the differences in the stability of OXA-48 and OXA-48Loop18, thermal denaturation by differential scanning calorimetry (DSC) was performed. Replacement of the β5-β6 loop of OXA-48 by the one of OXA-18 induced a decrease in the stability of the protein, which was reflected in a shift of the midpoint melting temperatures (Tm) from 56.8 °C to 41.1 °C.

OXA-48Loop18 crystallization and X-ray crystallography

OXA-48Loop18 structure was obtained with a 2.38 Å resolution (Table 3). The asymmetric unit contained two protein chains, A and B, with 252 residues each. They presented a classic class D β-lactamase fold, with an α-helical region and a mixed α-helix/β-sheet region. 96% of all residues were inside the favored regions of the Ramachandran plot, and 4% in the allowed regions. Clear electron density was observed throughout the protein (Fig. 2A), with average B-factors of 58.58 for the backbone of both chains, except for loops β5-β6 in chain A (average backbone B-factors: 121.22) and β7-α10 for both chains (average backbone B-factors of

109.74 and 105.34), where it was weaker. The structure contained several ordered water molecules, sulfate and fluoride from the crystallization solution, and glycerol from the cryoprotectant.

Excluding the exchanged loop, OXA-48Loop18 showed the same overall conformation as OXA-48 (PDB 4S2P)[22], with a Cα RMSD of 0.464 Å (Fig. S1). Active site residues (Fig. 2B) adopted the same conformation as in OXA-48. The grafted β5-β6 loop adopted a more relaxed and elongated conformation (Fig. 2C), extending the β5 and β6 strands, protruding away from the active site cavity. Residues 211 through 214, at the beginning of the β5-β6 loop, were displaced (Cα shifts of 0.56 Å, 0.75 Å, 3.12 Å and 6.64 Å, respectively, Fig. 3A), shifting closer to the Ω-loop and β6 strand. With the β5-β6 loop exchange, a cavity wall was lost with the lack of R214 (Fig. 3B), and the Y211T exchange created a shallow cleft close to the β5 strand. The sharp turn of the native β5-β6 loop imposed by the *cis*-peptide bond in OXA-48 by P217 does not occur in OXA-48loop18, where A222 took its place (Fig. 3A). In chain A the distal portion of β5-β6 loop folded back towards the Ω-loop, while in chain B it adopted an elongated conformation, extending away from the protein (Fig. S2 and Fig. 2C). In chain B, the loop replacement seemed to

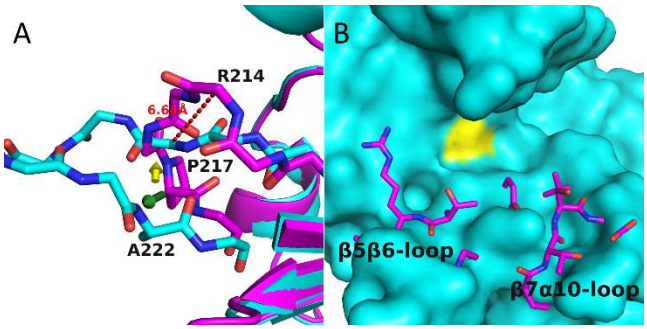

Figure 3. Superposition of OXA-48Loop18 and OXA-48 structures. A) Conformation of the β5-β6 loop of OXA-48 (magenta sticks) and OXA-48Loop18 (cyan sticks). Differences in conformation adopted translate into a 6.64 Å shift in the Cα of residue 214 (R214 in OXA-48). A yellow arrow points towards the *cis* peptide bond before P217 in OXA-48, and a green arrow towards the equivalent bond before A222 in OXA-48Loop18, which is in *trans* configuration. B) Active site cavity environment of OXA-48Loop18 (cyan surface), with OXA-48 (magenta sticks) superposed. Active site S70 is colored in yellow for reference. Notice how the OXA-48 structure emerges from the OXA-48Loop18 surface, demonstrating that the active site cavity of OXA-48 is narrower than that of OXA-48Loop18.

cause a slight shift in the adjacent β7-α10 loop. In chain A, this loop seemed to close on the active site cavity, aided by the unwinding of the N-terminus of α10 helix. Crystal packing seems to play a role in determining the conformations observed in the crystal. The β5-β6 loop of chain B contacts the α5-helix of chain A in a neighboring asymmetric unit. The fact that different conformations can be observed for the β5-β6 and β7-α10 loops while the enzyme's overall conformation is maintained, their weaker electron density, and the fact that native OXA-48 structures show a conserved conformation for these loops, all suggest that they may be more flexible in the OXA-48Loop18 structure than those of native OXA-48. Overall, the loop exchange seemed to cause the active site cavity to become wider (Fig. 3B). Homology modelling with Modeller [23] suggested the native β5-β6 loop of OXA-48 could not adopt the conformation observed in OXA-48Loop18 to widen the active site cavity, as it would require a *trans* E216-P217 bond, breaking the R214-D159 salt bridge [20], and breaking the last three hydrogen bonds between the β5 and β6 strands, given its short length.

S70 has been partially modelled as O-sulfo-L-serine (OSE) in both chains, with an occupancy of 0.5 (Fig. 2B). Other examples of serine sulfonylation can be found in the PDB (PDB codes 5V8D, 1EA7, 1YLN, 4HF7), but this is the first example on a β-lactamase. Another sulfate was modelled at 0.5 occupancy in the cavity, making hydrogen bonds with R255, T209, T211 and S118. Only the sulfate anion or the OSE is proposed to occupy the active site cavity at any given protein monomer in the crystal.

The serine sulfonylation seems to block the catalytic residue and active site cavity. However, the enzyme has been proven to be active by *in vivo* and *in vitro* assays, and the overall conformation is almost the same as that of native OXA-48. Previous reports have suggested it to be an *in-situ* modification that does not affect the protein conformation, occurring during crystallization from HEPES [24] or sulfate [25], in equilibrium with serine. It is therefore most likely the case here as well, as the modification did not occur until crystallization under these conditions was attempted and did not affect the biochemical or structural properties of the enzyme. Nevertheless, this modification is interesting from a crystallographic point of view given that it has never before been reported on a β-lactamase.

Covalent docking of β-lactams on OXA-48Loop18 and comparison with OXA-48

To explore the differences in K_m for ceftazidime and imipenem, acyl-enzyme complexes were created by covalent docking, for both enzymes. For the ceftazidime/OXA-48 complex, only unrealistic solutions were obtained with GOLD [26], showing severe clashes or an

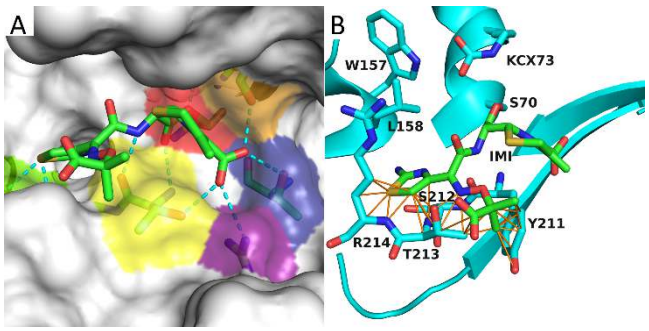

Figure 4. Docking of ceftazidime on OXA-48Loop18. A) Docking conformation of ceftazidime on OXA-48Loop18, making hydrogen bonds to S70 (in red), S118 (in orange), T209 (in blue), R255 (in purple), T211 (in yellow), and S213 (in green). The docking conformation is similar to the one observed for the complex of OXA-225 with ceftazidime (PDB code 4X55)[27]. B) Superposition of OXA-48 on OXA-48Loop18 with ceftazidime docked. Only OXA-48 (cyan sticks) and ceftazidime (green sticks) are shown for simplicity. Overlaps between the R1 sidechain of ceftazidime and residues 211-214 of OXA-48 can be observed, represented as thin orange lines that range from 2.0 to 0.6 Å. This implies that OXA-48 cannot accommodate ceftazidime as OXA-48Loop18 does.

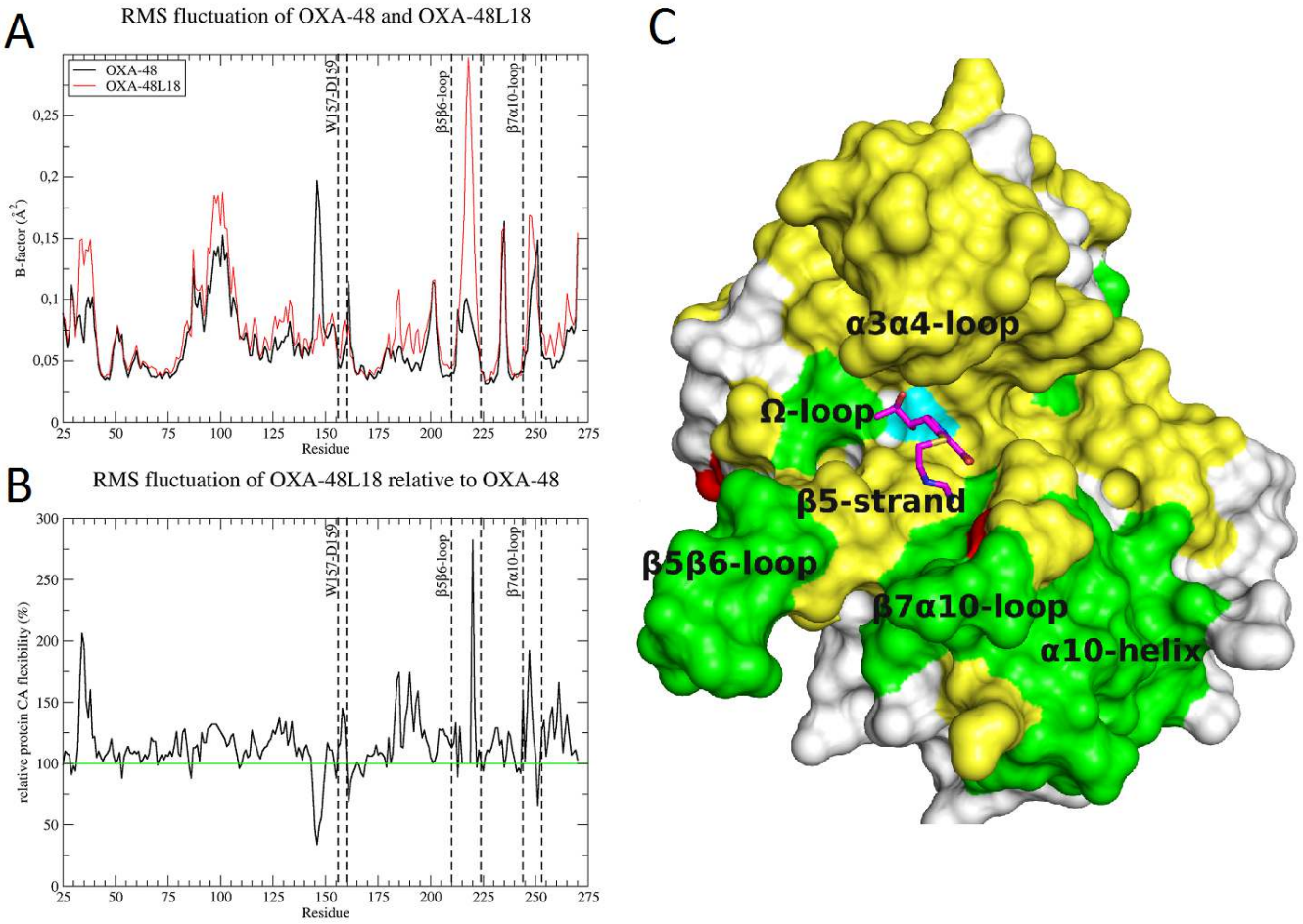

Figure 5. Flexibility of OXA-48Loop18. A) RMSF analysis of the OXA-48 and OXA-48Loop18 molecular dynamics simulations, expressed as Cα B-factors. OXA-48Loop18 shows an increased flexibility over most of the protein sequence. Notice the increase of flexibility on the β5-β6 and β7-α10 loops, and around L158 (regions delimited by dashed lines in the graph). B) Relative flexibility of OXA-48Loop18 compared to OXA-48. Notice the almost 50% increase in L158 flexibility, which may go unnoticed by looking at the absolute B-factor graph. C) Surface representation of OXA-48Loop18 with imipenem (magenta sticks), showing the parts with increased flexibility that surround and form the active site cavity. Increased flexibility has been depicted in yellow (moderate increase) and green (higher increase). Certain parts of the enzyme show decreased flexibility (colored red), such as the back of the Ω-loop and G251 in the β7-α10 loop. S70 surface is colored in cyan, for reference.

impossibly inverted orientation of the substrate. This was expected, as the OXA-48 cavity is supposed to be too small to bind ceftazidime. For OXA-48Loop18, ceftazidime could be docked in a coherent conformation with conserved interactions (Fig. 4A), similar to the OXA-160 and OXA-225 complexes (PDB codes 4X56 and 4X55) [27]. Superposing OXA-48 on the obtained complex illustrates how the native β5-β6 loop posed a steric impediment for binding ceftazidime (Fig. 4B), with severe clashes between the R1 substituent and Y211, S212, T213, and R214. Superposing OXA-48Loop18 on the available imipenem/OXA-48 complex (PDB 5QB4)[28] showed that minor clashes would occur between the R1 substituent and S118, V120, and L158 on OXA-48Loop18. Docking imipenem on OXA-48Loop18 showed a slight shift that would resolve the clashes.

Molecular dynamics simulations of OXA-48 and OXA-48Loop18

Molecular dynamics (MD) simulations of both enzymes were performed (10 ns each), both in the apo form and as covalent complexes with imipenem. Chain B was chosen for OXA-48Loop18, and chain A for OXA-48 (PDB 4S2K)[22]. OSE was replaced by SER70 in OXA-48Loop18, and ions and buffer molecules were removed from the starting structures. Simulations were run to assess if the loop exchange affected the dynamic behavior of the rest of the protein as well as itself, which may serve to explain the hydrolytic spectrum expansion. Simulations show that the grafted β5-β6 loop was more flexible than that of OXA-48, and may alternate between the two conformations observed in the crystal structure.

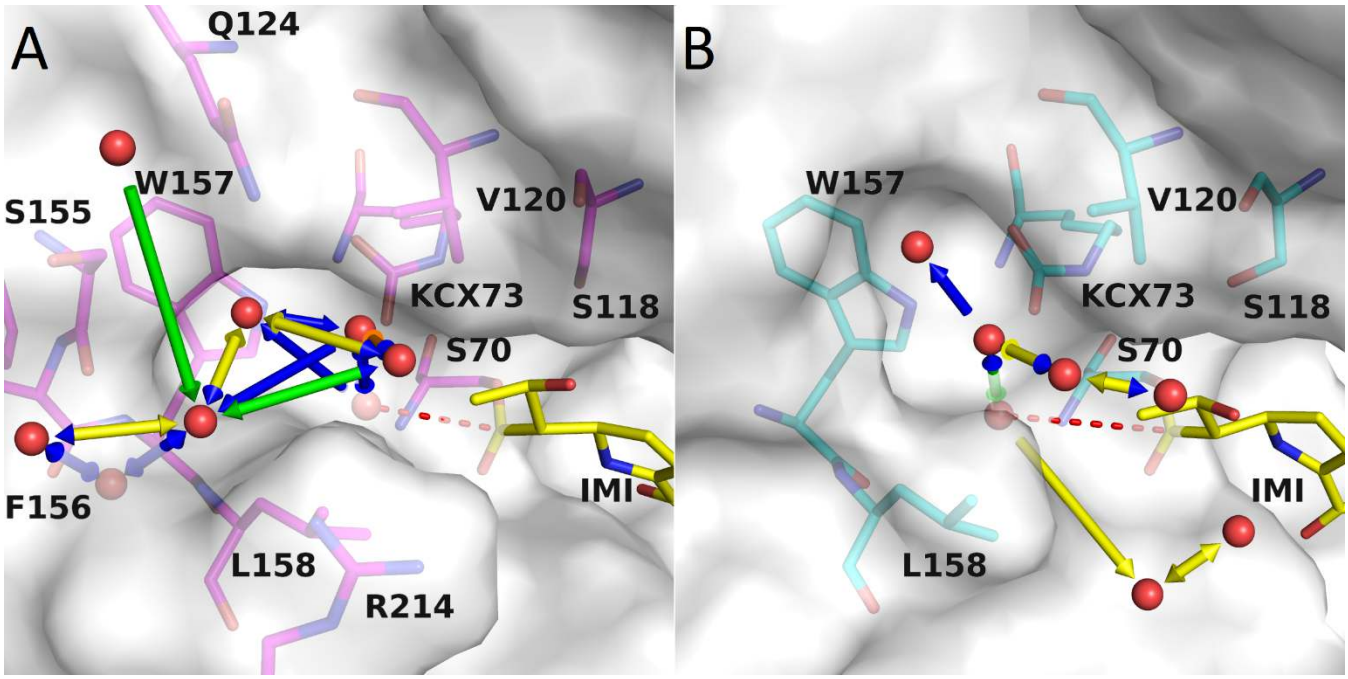

Figure 6. Water molecules flow into the active site cavity. A) In OXA-48/imipenem complex, the access to the hydrolytic water pocket in OXA-48 seems to be through a channel above L158, hopping on 4 to 5 conserved sites. B) In OXA-48Loop18/imipenem complex, the access to the hydrolytic water pocket seems to be more direct, hopping on 3 or 4 conserved sites, arriving from the β face of the substrate. Arrows represent water transitions (hops) between consensus positions. Arrow color is indicative of relative hopping rates: red, orange, yellow, green and blue, from faster to slower hopping rates. Two-headed arrows are colored as the faster rate arrow head is. Attacking water distance to scissile bond attack center is shown as red dashed lines. Imipenem is represented in yellow sticks.

Root mean square fluctuation (RMSF) analysis also revealed that other parts delimitating the cavity showed increased flexibility, such as the β7-α10 loop, K223 at the end of the β5-β6 loop (K218 in OXA-48), L158 on the Ω-loop, the α3-α4 loop, comprising I102 and W105 and the α4-α5 loop, comprising S118 and V120 (Fig. 5A and 5B).

MD simulations of the covalent complexes with imipenem were also performed. Results were coherent with the apoenzyme MD simulations: several parts of OXA-48Loop18 showed increased flexibility compared to OXA-48, even when covalently bound to imipenem: the α4-α5 loop, α3- α4 loop, the W157-L158-D159 portion of the Ω-loop, the whole β5 strand, the β5-β6 and β7-α10 loops, as well as other regions around the protein surface. The largest increases could be observed for L158, L214-K221 (β5-β6 loop), and N243-L254 (β7-α10 loop) (Fig. 5C).

The HOP package [29] was used to analyze the dynamic water network around the proteins during MD simulations (Fig. S3), to explore how the turnover rate of imipenem may be affected. The amount of consensus sites found for apo OXA-48 (186 sites) was significantly higher than for apo OXA-48Loop18 (52 sites), which may be related to the increased flexibility of OXA-48Loop18. However, a smaller difference between them (191 vs. 126) was observed when imipenem was bound. Also, hops between sites seemed to be more discrete for OXA-48Loop18 than for OXA-48, whether in the apo form or in complex with imipenem (Fig. S3).

The HOP analysis also revealed conserved water positions in the active site cavity of OXA-48, and how these positions were displaced upon binding of imipenem (Fig. S4), which supports the hypothesis that the R1 group of carbapenems pushes the attacking water away from an optimal attacking position [30]. HOP analysis could also elucidate the path for accession of a water molecule to the hydrolytic water position, which could affect the likelihood of this position being populated, and therefore the turnover rate. In the case of OXA-48 (Fig. 6A) water molecules accessing this cavity could originate from the bulk solvent or conserved positions around the Ω-loop surface and were most likely to enter through a channel between V120, L158 and Q124, by hydrogen bonding the following residues: R214 sidechain, S155 sidechain or F156 backbone, Q124 sidechain, W157 sidechain, and finally KCX73, about 2 Å above the hydrolytic water pocket. The final access to this pocket seemed to be allowed by the movement of the L158 sidechain and the imipenem's R1 sidechain. These movements may be directly influenced by the loop exchanged, as it has been proposed that a hydrophobic patch between the β5-β6 loop and the Ω-loop may interact with the R1 sidechain to help it turn [20], and a similar interaction was proposed for L166 in the case of OXA-23/meropenem complex [31]. During the MD simulation of OXA-48 it was also observed that S118 could turn and make a hydrogen bond with the R1 sidechain, which is possibly participating in this turning event.

In the case of OXA-48Loop18, the access to the active site seemed to be through a different path (Fig. 6B), not hopping over the protein surface like in OXA-48. The R214 sidechain at the edge of the entering channel was not present in this β5-β6 loop, and the backbone of the Ω-loop was more flexible (Fig. 5B). Water molecules reaching the hydrolytic water pocket seemed to originate from the bulk solvent close to the α face of imipenem, hopping through two consensus positions next to the R1 sidechain, later binding KCX73 and then accessing the pocket below. Notably, unlike for the

OXA-48/imipenem complex MD simulation, an exit path was observed in the case of OXA-48Loop18/imipenem complex for the hydrolytic water, passing between L158, imipenem, and S212 (Fig. 6B).

Another factor influencing the turnover rate, evidenced by the HOP analysis, was the likelihood of a water molecule being in the right position to be activated and to attack the scissile bond. In the case of OXA-48 and OXA-48Loop18 with imipenem, the average position adopted by the hydrolytic water molecule inside the pocket and the average conformation of the covalently bound imipenem seemed to be different (Fig. 7). For OXA-48, the water molecule average position had an occupancy of 0.60, and is situated 3.67 Å away from the β-lactam carbon, at an angle of 70.8° from the ester bond plane. For OXA-48Loop18, the same pocket contained a water molecule average position with an occupancy of 0.52, positioned 4.54 Å away from the β-lactam carbon, and at an angle of 59.0° from the ester bond plane.

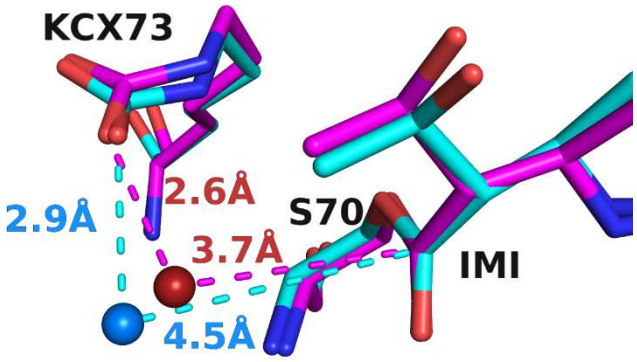

Figure 7. Conserved water site in the hydrolytic water pocket. Conserved water position as determined by HOP analysis for OXA-48/imipenem complex (magenta) and OXA-48Loop18/imipenem complex (cyan). The conserved position for the OXA-48Loop18 enzyme is farther from both the activating KCX73 and the scissile bond, and at a less favorable angle (59.0° instead of 70.8°). Only imipenem, KCX73 and S70 are shown for simplicity.

Discussion

The β5-β6 loop appears to have a profound influence on the hydrolytic profile of class D β-lactamases [20,21]. Deletions on this loop and loop exchange experiments have already been described to alter the hydrolytic profile, being able to turn non-carbapenemases into carbapenemases, as well as the opposite [7,21]. The mechanisms by which β-lactamases achieve this can depend on the enzyme characteristics and the substrates in question. Substitutions of residues that may pose a steric impediment for the binding of substrates for smaller or more flexible residues can also occur, as well as mutations that may allow favorable new interactions with a certain substrate to be made [32]. The β5-β6 loop of OXA-48 has already been proposed to be an impediment for the binding of big substrates such as expanded-spectrum cephalosporins, as well as intervening in the turnover rate of carbapenems by interacting with the R1 sidechain to facilitate rotation and allow the water molecule to perform deacylation [20].

In this work, we successfully transferred the β5-β6 loop of an expanded-spectrum cephalosporinase, OXA-18, to the carbapenemase OXA-48. Unexpectedly, the hybrid enzyme OXA-48Loop18 was able to hydrolyze not only cephalosporins, but still carbapenems as well (alhough with a lower k_{cat}), even though the β5-β6 loop was longer and its sequence quite different from that of OXA-48. These results give further evidence not only of the participation of the β5-β6 loop in the carbapenem hydrolysis [20,21] but also of its influence on the hydrolysis of bulkier β-lactams (e. g. ceftazidime).

According to the stability-activity tradeoff model, larger substrates are recognized by the introduction of stability defects that increase the ground-state size of the enzyme active site or its ability to flex when confronted by the larger substrates, facilitating the hydrolysis of the bulkier substrates [15,33]. Here, the grafted loop allows the enzyme to hydrolyze a larger substrate, causes a loss in the thermal-stability of the protein, and a higher degree of flexibility is observed in the MD simulations. Therefore, this tradeoff seems to be playing a role in the hydrolytic profile expansion as well. However, more localized effects could be taking place as well. The increased flexibility of L158, for example, may also collaborate in admitting larger substrates into the active site cavity of OXA-48Loop18 [27].

We also present here crystallographic and molecular modeling results that support the hypothesis that the β5-β6 loop of OXA-48 is probably an impediment for the binding of ceftazidime or other bulky substrates, such as aztreonam, regarding mostly the R1 substituent of β-lactams which is positioned towards the β5-β6- and Ω-loops. Indeed, these two substrates present different R2 substituents but the same R1 sidechain, and their interaction with the enzyme seems to be affected in a similar way. This steric impediment derives not only from the presence of R214 and other sidechains, but also from the backbone conformation that the whole β5-β6 loop adopts, caused by its shortness, the turn imposed by the *cis* bond of P217 and the R214-D159 salt bridge. These are not present in the longer, grafted loop. It therefore adopts a more relaxed conformation, not causing these unfavorable interactions, thus explaining the extended hydrolytic profile observed for this mutant [34]. It is noteworthy that, compared to ceftazidime, there is a difference in behavior respecting other cephalosporins with a similar but more compact R1 substituent such as cefotaxime or cefepime. These seem to fit OXA-48 already, and so their affinity is almost unaffected by the loop exchange. Possibly, they fit into OXA-48 with the more compact R1 substituent in a different orientation as ceftazidime, and slightly shifted, avoiding the steric impediment ceftazidime seems to suffer.

The K_m of imipenem, a relatively smaller substrate, is also affected by the loop exchange. Superposition of the OXA-48/imipenem complex (PDB 5QB4)[28] on OXA-48Loop18 shows slight clashes between the imipenem and L158, V120 and S118 sidechains. Covalent docking of imipenem on OXA-48Loop18 is highly similar but slightly shifted, to avoid these light overlaps. But the 10-fold increase in K_m may also be due to the same widening and increased flexibility of the active site cavity that now allow bulkier substrates to enter. Unlike for ceftazidime, it may have a negative impact on the affinity for a small substrate such as imipenem, for which the OXA-48 structure with its narrower cavity was already well adapted.

The loop exchange affects turnover rates as well. The 6-α-hydroxyethyl substituent of carbapenems is supposed to prevent the attacking water from hydrolyzing the acyl-enzyme complex, and in the case of OXA-48 it has been proposed that the β5-β6 loop aids to rotate this group, allowing the water molecule to approach the scissile bond [20]. With the loop exchange, not only is the primary sequence different (T213 is replaced by S213), but the conformation it adopts is different too, so it is possible that it can no longer provide a hydrophobic patch to aid the R1 group to rotate, which probably impacts the turnover rate for imipenem. Another factor influencing turnover rate is how likely it is that a water molecule will hydrolyze the acyl-enzyme complex. In this respect, the HOP analysis shows several interesting differences between OXA-48 and OXA-48Loop18 acyl-enzyme complexes with imipenem, concerning the dynamic water network behavior in the active site. The route a water molecule is most likely to follow to enter the active site cavity on both enzymes is different, which can affect the availability of an attacking water molecule in the active site. Furthermore, the hop that allows the attacking water molecule to exit its pocket in the OXA-48Loop18 simulation may also contribute to the decrease of turnover rate for imipenem. At the same time, it probably alters the hydrogen bond network between water molecules and residues inside the active site, which can influence the position and energy of the attacking water. The attacking water in particular presents an equilibrium position relative to the acyl moiety that is different in both enzymes. It is closer and at a better angle for attack in OXA-48, which may explain the higher turnover rates compared to OXA-48Loop18. The β5-β6 loop does not seem to interact directly with the hydrolytic water molecule, but it may exert its effect by changing the hydrogen bond network along with the water path alterations proposed by the HOP analysis, or via neighboring residues and groups that do contact the hydrolytic water. The β5-β6 loop has been proposed to interact with the R1 substituent on carbapenems [20], and the latter with the hydrolytic water [30]. The loop exchange also causes changes in the flexibility of L158 and the position of the β5 strand, which contacts A69, both residues neighboring the attacking water.

Considering that the entire β5-β6 loop of OXA-48 was replaced for a 5 AA longer one, with a different amino acid composition, and that imipenem hydrolysis was still observed, our results suggest that the presence of the exact β5-β6 loop of OXA-48 or similar is not absolutely fundamental for the hydrolysis of carbapenems. Its three-dimensional conformation however, may be. It was shown that OXA-48 and OXA-24, both CHDLs, present the same conformation of the β5-β6 loop [20]. The same situation is observed in the crystal structure of OXA-181 and OXA-245 [15]. At the same time, the superposition of OXAs with expanded-spectrum cephalosporinase activity and non-carbapenemase activity shows heterogeneity in the disposition of the β5-β6 loop (Fig. 8). This might suggest, firstly, that only the OXAs with the β5- β6 loop in the OXA-48 loop conformation, or close to it, would be able to hydrolyze carbapenems efficiently, while OXAs presenting different loop conformations would hydrolyze expanded spectrum cephalosporins. Secondly, there are loop sequences that produce intermediate states (expanded hydrolysis spectrum), such as for our hybrid protein, that can hydrolyze both types of substrates (although with a lower k_{cat} for carbapenems), with a β5-β6 loop quite different in primary sequence from the one of OXA-48, but more similar in orientation to it than the β5-β6 loop of other OXAs, such as OXA-10. Lastly, if only the modification of the β5-β6 loop of OXA-48 is sufficient for it to start hydrolyzing expanded-spectrum cephalosporins, this suggests that the rest of the enzyme active site residues present a pertinent configuration and conformation for the acylation and deacylation process of cephalosporins.

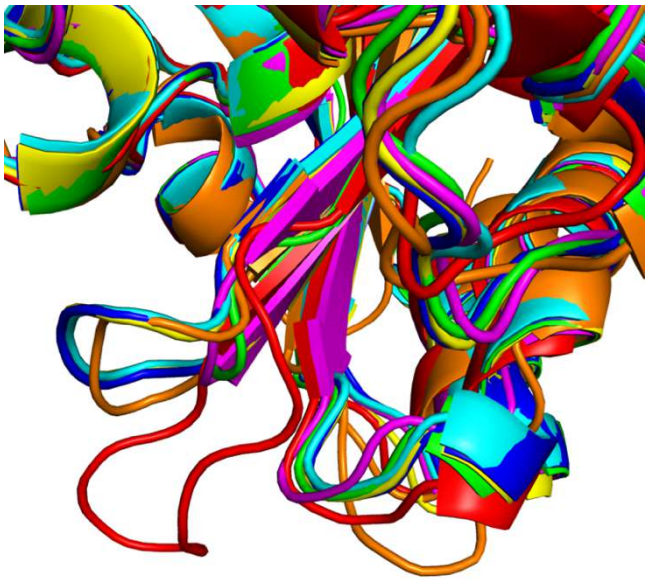

Figure 8. β5-β6 loop conformation of OXAs with different hydrolytic profiles. β5-β6 loop conformation adopted by different OXA type enzymes. Red: OXA-10, green: OXA-163, blue: OXA-181, yellow: OXA-245, magenta: OXA-405, cyan: OXA-48, orange: OXA-51. Of note the almost identical conformation of the OXA-181, OXA-245 and OXA-48 loops.

Our results provide further evidence that the β5-β6 loop of OXA-48 would influence the hydrolytic profile, presenting a steric impediment for cephalosporins or other bulky substrates [34]. Moreover, the loop exchange seems to have an effect on k_{cat}, for imipenem at least, by altering the attacking water occupancy within the pocket, and its position relative to the substrate. Subsequent experiments would provide further evidence to corroborate how the β5-β6 loop sequence affects the β-lactamase function, in terms of turnover rate and affinity for its substrates.

Methods

Bacterial strains.

K. pneumoniae 11978 was used as a reference strain for OXA-48 cloning experiments [8]. *P. aeruginosa* Mus was used as a reference strain for OXA-18 cloning experiments [19].

Antimicrobial agents, susceptibility testing.

Antimicrobial susceptibilities were determined by disk diffusion technique on Mueller-Hinton agar (Bio-Rad, Marnes-La-Coquette, France) and interpreted according to the EUCAST breakpoints, updated in 2018 (http://www.eucast.org). Minimal inhibitory concentration (MIC) values were determined using the Etest technique (BioMérieux, Paris, France).

PCR and cloning experiments.

Whole-cell DNAs of *K. pneumoniae* 11978 isolate and of *P. aeruginosa* Mus were extracted using the QIAamp DNA minikit (Qiagen, Courtaboeuf, France) and were used as template for PCR using the following primers: preOXA-48A (5'-TATATTGCATTAAGCAAGGG-3'), cloningOXA-48B (5'-AAAAGGATCCCTAGGGAATAATTTTTTCCTGTTTGAGC A -3'), preOXA-18Fw (5'-AAAACATATGCAACGGAGCCTGT-3') and preOXA-18Rv (5'-AAAAGGATCCTCAGAAGTTTTCCG ACAGG-3') in order to amplify bla_{OXA-48} and bla_{OXA-18} genes, respectively. The hybrid gene of OXA-48Loop18 was constructed by overlapping PCR with partially overlapping primers. The first PCRs were done using preOXA-48A primer with P_inside_48Loop18_B (5'-ACCGGTTCGCTT TCCGATGCCAAGGGCGGCAAGGCGAAGATT GCTGGTGGGTC-3') and cloning OXA-48B primer in combination with P_inside_48Loop18_B (5'-ACCGGTTCGCTTTCCGATGCCAA GGGCGGCAAGGCGAAGATTGGCTGGTGGGTC-3'). The products of these PCR were then purified using GeneJET PCR Purification Kit (Thermo Scientific™, Montigny-le-Bretonneux, France) and mixed for being used as template for a second PCR using the primers preOXA-48A and cloningOXA-48B. The amplicons obtained in all cases were then cloned into the pCR®-Blunt II-TOPO® plasmid (Invitrogen, Illkirch, France) downstream from the pLac promoter, in the same orientation. The recombinant pTOPO-OXA plasmids were electroporated into the *E. coli* TOP10 strain. The electroporants were plated on a TSA plate containing kanamycin (50 ug/ml). The $bla_{OXA-48Loop18}$ gene fragment corresponding to the mature β-lactamase was cloned into the expression vector pET41b (+) (Novagen, VWR International, Fontenay-sous-Bois, France) using the PCR generated fragment with primers INF-OXA-48Fw (5'-AAGGAGATATACATATGGTAGCAAAGGAATGGCAAG-3') and INF-OXA-48Rv (5'-GGTGGTGGTGCTCGAAGGGAATAATTTTTTCCTGTTTG AG-3') and the NEBuilder® HiFiDNA Assembly Cloning Kit (New England BioLabs®Inc, United Kingdom), following the manufacturer's instructions. Recombinant plasmid pET41-OXA-48Loop18 was transformed into chemocompetent *E. coli* strain BL21 (DE3).

Recombinant plasmids were extracted using the Qiagen miniprep kit and both strands of the inserts were sequenced using M13 primers, for the pCR®-Blunt II-TOPO® plasmid (Invitrogen, Illkirch, France), and T7 primers, for pET41b(+) (Novagen, VWR International, Fontenay-sous-Bois, France), with an automated sequencer (ABI Prism 3100; Applied Biosystems). The nucleotide sequences were analyzed using software available at the National Center for Biotechnology Information website (http://www.ncbi.nlm.nih.gov).

β-Lactamase purification.

An overnight culture of *E. coli* strain BL21 (DE3) harboring pET41b-OXA-48Loop18 was used to inoculate 2 L of LB broth containing 50 mg/L kanamycin. Bacteria were cultured at 37°C until reaching an OD of 0.6 at 600 nm. Expression of the OXA-48Loop18 was induced overnight at 25°C with 0.2 mM IPTG, as previously described [35]. OXA-48Loop18 was purified in one step pseudo-affinity chromatography using a NTA-Nickel column (GE Healthcare, Freiburg, Germany) [35]. Protein purity was estimated by SDS–PAGE, pure fractions were pooled and dialyzed against 20mM Hepes SO_4K_2 50 mM buffer (pH 7) and concentrated by using Vivaspin® columns (GE Healthcare, Freiburg, Germany). Protein concentration was determined by Bradford Protein assay (Bio-Rad, Marnes-La-Coquette, France) [36].

Steady-state kinetic parameters.

Kinetic parameters of purified OXA-48Loop18 were determined at 30°C in 100 mM sodium phosphate buffer (pH 7) as previously described [35,37].

Thermostability analysis.

Melting temperature was determined by MicroCal PEAQ-DSC Automated (Malvern). Purified proteins (350 µl at 1 mg/ml) were analyzed. The temperature of sample holding compartment was set at 5°C to maintain the integrity of sample prior to experiment. Samples were heated from 20°C to 110°C using a 1°C/min rate. A pressure of nitrogen gas (60 psi) was applied to suppress boiling of samples. The thermal behavior of samples was recorded and analyzed using the MicroCal PEAQ-DSC software.

Protein crystallization and X-ray crystallography.

OXA-48Loop18 (26.8 $mg.ml^{-1}$) crystalized in a 2.2 M ammonium sulfate, 0.2 M ammonium fluoride solution, at room temperature (pH ~5.3). The crystal was transferred to a cryo-protectant solution (mother liquor plus 25% glycerol) and flash-frozen in liquid nitrogen. Diffraction data was collected at 100 K in a nitrogen cryostream on the PROXIMA1 beamline at the SOLEIL synchrotron (Saint-Aubin, France). The data were indexed and integrated with XDS [38] *via* the *XDSME* script (https://github.com/legrandp/xdsme [39]).

Data scaling was performed using AIMLESS [40] from the CCP4 suite [41]. Data collection and refinement statistics are given in Table 3. The structure was solved by molecular replacement using *MrBUMP* [42], with OXA-48 (PDB 4S2K; 91% identity)[22], as search model. The model was rebuilt manually in Coot [43] and then refined using BUSTER-TNT [44] with local noncrystallographic symmetry (NCS) restraints and a translation–libration–screw (TLS) description of B factors [45]. The quality of the final refined model was assessed using MolProbity [46].

Structure analysis and covalent docking.

UCSF Chimera package [47] was used for structure comparison and docking results analysis. Covalent docking was performed using the GOLD suite (CCDC) [26] and the GoldScore scoring function, with the structure 4S2K[22] as receptor and the binding site defined as a 20 Å radius

Table 3. Crystallography data collection and refinement statistics.

Data collection	

Space group	$P\,2_1\,3$
Cell dimensions	
a, b, c (Å)	126.65, 126.65, 126.65
α, β, γ (°)	90, 90, 90
Resolution (Å)	19.78-2.38
Rmeas	14.6%
I/σ(I)	1.41 (at 2.38Å)
Completeness (%)	99.3
Redundancy	16.3
Refinement	
Resolution range (Å)	19.78-2.38
No. unique reflections	27,144
R_{work}/R_{free}	17.1%/21.4%
No. non-hydrogen atoms	
Protein	4,088
Water	103
Ligand/Ions	100
Total	4,291
Average B, all atoms (Å^2)	61.14
Protein	61.02
Water	56.44
Ligand/Ions	70.93
Root mean squared deviations	
Bond lengths (Å)	0.01
Bond angles (°)	1.11

sphere centred on the OG atom of S70. Ligand structures were generated with 3D Structure Generator CORINA Classic version 3.60 (Molecular Networks GmbH, Nuremberg, Germany) and the covalent link was made with the OG atom of S70.

Molecular dynamics simulations and HOP analysis.

Molecular dynamics simulations were performed with Gromacs version 4.6 [48] using the OPLS-AA force field [49]. Force field parameters for

covalently-bound imipenem were built using a modified version of our in-house MOL2FF package. Crystallographic waters were kept for the starting structure. The protein was centered in a cubic periodic box, with at least 1.0 nm on each side. The simulation box was then filled with TIP4P water molecules and the system neutralized with Na+ and Cl– ions until reaching the physiological ionic strength (150 mM). Each system was energy-minimized until convergence using a steepest descents algorithm. Molecular dynamics with position restraints was then performed for 200 ps, followed by the production run of 10 ns. During the position restraints and production runs, the Parrinello–Rahman method was used for pressure coupling[50], and the temperature was coupled using the Nosé–Hoover method at 300 K[51,52]. Electrostatics were calculated with the particle-mesh Ewald method[53]. The P-LINCS algorithm was used to constrain bond lengths, and a time step of 2 fs was used throughout[54].

HOP software version 0.4.0 alpha2 (https://github.com/Becksteinlab/hop) [29] was used for water molecule dynamics analysis. The HOP package analyses MD trajectories, aligning the structures from each frame of the simulation, and statistically determining the average positions where water molecules consistently interact with the structure occupying a certain position longer than in the bulk solvent, to determine consensus water sites, along with their frequency of occupancy. The software also tracks individual water molecules throughout the simulation to determine how they flow through these positions, and to/from bulk solvent, to determine a "hop" rate for each jump connecting any two consensus positions. This kind of analysis can be used to identify stabilized water molecules, similar to analyzing crystallographic water positions in the X-ray structures, but independent of crystallography resolution, and taking structure flexibility into account. For more details refer to the original publication[29].

ASSOCIATED CONTENT

Data availability.

OXA-48Loop18 structure has been deposited to the PDB, accession code 6HOO.

Supporting Information. This material is available free of charge via the Internet at http://pubs.acs.org."

- Fig. S1. Structure of OXA-48 and β5-β6 loop replacement.
- Fig. S2. Conformation of β5-β6 loop in OXA-48Loop18.
- Fig. S3. Water networks around OXA-48 and OXA-48Loop18.
- Fig. S4. Displacement of active site water molecules.

AUTHOR INFORMATION

Corresponding Authors

* Thierry Naas, thierry.naas@aphp.fr, and Bogdan I. Iorga, bogdan.iorga@cnrs.fr.

Author Contributions

# These authors contributed equally.

Funding Sources

This work was supported by the Assistance Publique – Hôpitaux de Paris (AP-HP), the University Paris-Sud, the Laboratory of Excellence in Research on Medication and Innovative Therapeutics (LERMIT) supported by a grant from the French National Research Agency [ANR-10-LABX-33], by the Joint Programming Initiative on Antimicrobial Resistance (JPIAMR) DesInMBL [ANR-14-JAMR-002], and by DIM Malinf, Ile de France, for LD's PhD fellowship.

ACKNOWLEDGMENT

We acknowledge SOLEIL for provision of synchrotron radiation facilities (proposal ID BAG20170782) in using PROXIMA beamlines. This work has benefited from the platform and expertise of the Macromolecular interactions measurements Platform of I2BC and from the I2BC crystallization platform, supported by FRISBI ANR-10-INSB-05-01.

REFERENCES

(1) Naas, T.; Nordmann, P. (1999) OXA-Type β-Lactamases. *Curr. Pharm. Des., 5* (11), 865–879.

(2) Naas, T.; Oueslati, S.; Bonnin, R. A.; Dabos, M. L.; Zavala, A.; Dortet, L.; Retailleau, P.; Iorga, B. I. (2017) Beta-Lactamase Database (BLDB) – Structure and Function. *J. Enzyme Inhib. Med. Chem., 32*

(1), 917–919 DOI 10.1080/14756366.2017.1344235.

(3) Poirel, L.; Naas, T.; Nordmann, P. (2010) Diversity, Epidemiology, and Genetics of Class D β-Lactamases. *Antimicrob. Agents Chemother.*, *54* (1), 24–38 DOI 10.1128/AAC.01512-08.

(4) El Garch, F.; Bogaerts, P.; Bebrone, C.; Galleni, M.; Glupczynski, Y. (2011) OXA-198, an Acquired Carbapenem-Hydrolyzing Class D Beta-Lactamase from Pseudomonas Aeruginosa. *Antimicrob. Agents Chemother.*, *55* (10), 4828–4833 DOI 10.1128/AAC.00522-11.

(5) Docquier, J.-D.; Mangani, S. (2016) Structure-Function Relationships of Class D Carbapenemases. *Curr. Drug Targets*, *17* (9), 1061–1071 DOI 10.2174/1389450116666150825115824.

(6) Poirel, L.; Potron, A.; Nordmann, P. (2012) OXA-48-like Carbapenemases: The Phantom Menace. *J. Antimicrob. Chemother.*, *67* (7), 1597–1606 DOI 10.1093/jac/dks121.

(7) Oueslati, S.; Nordmann, P.; Poirel, L. (2015) Heterogeneous Hydrolytic Features for OXA-48-like β-Lactamases. *J. Antimicrob. Chemother.*, *70* (4), 1059–1063 DOI 10.1093/jac/dku524.

(8) Poirel, L.; Héritier, C.; Tolün, V.; Nordmann, P. (2004) Emergence of Oxacillinase-Mediated Resistance to Imipenem in Klebsiella Pneumoniae. *Antimicrob. Agents Chemother.*, *48* (1), 15–22 DOI 10.1128/AAC.48.1.15-22.2004.

(9) Aubert, D.; Naas, T.; Héritier, C.; Poirel, L.; Nordmann, P. (2006) Functional Characterization of IS1999, an IS4 Family Element Involved in Mobilization and Expression of β-Lactam Resistance Genes. *J. Bacteriol.*, *188* (18), 6506–6514 DOI 10.1128/JB.00375-06.

(10) Potron, A.; Poirel, L.; Rondinaud, E.; Nordmann, P. (2013) Intercontinental Spread of OXA-48 Beta-Lactamase-Producing Enterobacteriaceae over a 11-Year Period, 2001 to 2011. *Euro Surveill.*, *18* (31), 20549 DOI 10.2807/1560-7917.ES2013.18.31.20549.

(11) Dortet, L.; Cuzon, G.; Ponties, V.; Nordmann, P. (2017) Trends in Carbapenemase-Producing Enterobacteriaceae, France, 2012 to 2014. *Euro Surveill.*, *22* (6), 30461 DOI 10.2807/1560-7917.ES.2017.22.6.30461.

(12) Cuzon, G.; Ouanich, J.; Gondret, R.; Naas, T.; Nordmann, P. (2011) Outbreak of OXA-48-Positive Carbapenem-Resistant Klebsiella Pneumoniae Isolates in France. *Antimicrob. Agents Chemother.*, *55* (5), 2420–2423 DOI 10.1128/AAC.01452-10.

(13) Oueslati, S.; Dabos, M. L.; Zavala, A.; Iorga, B. I.; Naas, T. (2018) A Greater than Expected Variability among OXA-48-like Carbapenemases. *Rom. Arch. Microbiol. Immunol.*, *77* (2), 117–122.

(14) Poirel, L.; Castanheira, M.; Carrër, A.; Rodriguez, C. P.; Jones, R. N.; Smayevsky, J.; Nordmann, P. (2011) OXA-163, an OXA-48-Related Class D β-Lactamase with Extended Activity Toward Expanded-Spectrum Cephalosporins. *Antimicrob. Agents Chemother.*, *55* (6), 2546–2551 DOI 10.1128/AAC.00022-11.

(15) Lund, B. A.; Thomassen, A. M.; Carlsen, T. J. O.; Leiros, H. K. S. (2017) Structure, Activity and Thermostability Investigations of OXA-163, OXA-181 and OXA-245 Using Biochemical Analysis, Crystal Structures and Differential Scanning Calorimetry Analysis. *Acta Crystallogr. Sect. F, Struct. Biol. Commun.*, *73* (Pt 10), 579–587 DOI 10.1107/S2053230X17013838.

(16) Gomez, S.; Pasteran, F.; Faccone, D.; Bettiol, M.; Veliz, O.; De Belder, D.; Rapoport, M.; Gatti, B.; Petroni, A.; Corso, A. (2013) Intrapatient Emergence of OXA-247: A Novel Carbapenemase Found in a Patient Previously Infected with OXA-163-Producing Klebsiella Pneumoniae</Em>. *Clin. Microbiol. Infect.*, *19* (5), E233–E235 DOI 10.1111/1469-0691.12142.

(17) Dortet, L.; Oueslati, S.; Jeannot, K.; Tandé, D.; Naas, T.; Nordmann, P. (2015) Genetic and Biochemical Characterization of OXA-405, an OXA-48-Type Extended-Spectrum β-Lactamase without Significant Carbapenemase Activity. *Antimicrob. Agents Chemother.*, *59* (7), 3823–3828 DOI 10.1128/AAC.05058-14.

(18) Oueslati, S.; Retailleau, P.; Marchini, L.; Dortet, L.; Bonnin, R. A.; Iorga, B. I.; Naas, T. (2019) Biochemical and Structural Characterization of OXA-405, an OXA-48 Variant with Extended-Spectrum β-Lactamase Activity. *Microorganisms*, *8* (1), 24 DOI 10.3390/microorganisms8010024.

(19) Philippon, L. N.; Naas, T.; Bouthors, A. T.; Barakett, V.; Nordmann, P. (1997) OXA-18, a Class D Clavulanic Acid-Inhibited Extended-Spectrum Beta-Lactamase from Pseudomonas Aeruginosa. *Antimicrob. Agents Chemother.*, *41* (10), 2188–2195 DOI 10.1128/AAC.41.10.2188.

(20) Docquier, J.-D.; Calderone, V.; De Luca, F.; Benvenuti, M.; Giuliani, F.; Bellucci, L.; Tafi, A.; Nordmann, P.; Botta, M.; Rossolini, G. M.; Mangani, S. (2009) Crystal Structure of the OXA-48 β-Lactamase Reveals Mechanistic Diversity among Class D Carbapenemases. *Chem. Biol.*, *16* (5), 540–547 DOI 10.1016/J.CHEMBIOL.2009.04.010.

(21) De Luca, F.; Benvenuti, M.; Carboni, F.; Pozzi, C.; Rossolini, G. M.; Mangani, S.; Docquier, J.-D. (2011) Evolution to Carbapenem-Hydrolyzing Activity in Noncarbapenemase Class D β-Lactamase OXA-10 by Rational Protein Design. *Proc. Natl. Acad. Sci. U. S. A.*, *108* (45), 18424–18429 DOI 10.1073/pnas.1110530108.

(22) King, D. T.; King, A. M.; Lal, S. M.; Wright, G. D.; Strynadka, N. C. J. (2015) Molecular Mechanism of Avibactam-Mediated β-Lactamase Inhibition. *ACS Infect. Dis.*, *1* (4), 175–184 DOI 10.1021/acsinfecdis.5b00007.

(23) Eswar, N.; Webb, B.; Marti-Renom, M. A.; Madhusudhan, M. S.; Eramian, D.; Shen, M.; Pieper, U.; Sali, A. (2006) Comparative Protein Structure Modeling Using Modeller. *Curr. Protoc. Bioinforma.*, *15* (1), 5.6.1-5.6.30 DOI 10.1002/0471250953.bi0506s15.

(24) Almog, O.; González, A.; Klein, D.; Greenblatt, H. M.; Braun, S.; Shoham, G. (2003) The 0.93 Å Crystal Structure of Sphericase: A Calcium-Loaded Serine Protease from Bacillus Sphaericus. *J. Mol. Biol.*, *332* (5), 1071–1082 DOI 10.1016/J.JMB.2003.07.011.

(25) Sychantha, D.; Little, D. J.; Chapman, R. N.; Boons, G.-J.; Robinson,

H.; Howell, P. L.; Clarke, A. J. (2017) PatB1 Is an O-Acetyltransferase That Decorates Secondary Cell Wall Polysaccharides. *Nat. Chem. Biol.*, *14* (1), 79–85 DOI 10.1038/nchembio.2509.

(26) Verdonk, M. L.; Cole, J. C.; Hartshorn, M. J.; Murray, C. W.; Taylor, R. D. (2003) Improved Protein-Ligand Docking Using GOLD. *Proteins Struct. Funct. Bioinforma.*, *52* (4), 609–623 DOI 10.1002/prot.10465.

(27) Mitchell, J. M.; Clasman, J. R.; June, C. M.; Kaitany, K.-C. J.; LaFleur, J. R.; Taracila, M. A.; Klinger, N. V.; Bonomo, R. A.; Wymore, T.; Szarecka, A.; Powers, R. A.; Leonard, D. A. (2015) Structural Basis of Activity against Aztreonam and Extended Spectrum Cephalosporins for Two Carbapenem-Hydrolyzing Class D β-Lactamases from Acinetobacter Baumannii. *Biochemistry*, *54* (10), 1976–1987 DOI 10.1021/bi501547k.

(28) Akhter, S.; Lund, B. A.; Ismael, A.; Langer, M.; Isaksson, J.; Christopeit, T.; Leiros, H.-K. S.; Bayer, A. (2018) A Focused Fragment Library Targeting the Antibiotic Resistance Enzyme - Oxacillinase-48: Synthesis, Structural Evaluation and Inhibitor Design. *Eur. J. Med. Chem.*, *145*, 634–648 DOI 10.1016/J.EJMECH.2017.12.085.

(29) Beckstein, O.; Michaud-Agrawal, N.; Woolf, T. B. (2009) Quantitative Analysis of Water Dynamics in and near Proteins. *Biophys. J.*, *96* (3), 601a DOI 10.1016/j.bpj.2008.12.3147.

(30) Taibi, P.; Mobashery, S. (1995) Mechanism of Turnover of Imipenem by the TEM β-Lactamase Revisited. *J. Am. Chem. Soc.*, *117* (29), 7600–7605 DOI 10.1021/ja00134a003.

(31) Smith, C. A.; Antunes, N. T.; Stewart, N. K.; Toth, M.; Kumarasiri, M.; Chang, M.; Mobashery, S.; Vakulenko, S. B. (2013) Structural Basis for Carbapenemase Activity of the OXA-23 β-Lactamase from Acinetobacter Baumannii. *Chem. Biol.*, *20* (9), 1107–1115 DOI 10.1016/j.chembiol.2013.07.015.

(32) Dabos, L.; Jousset, A. B.; Bonnin, R. A.; Fortineau, N.; Zavala, A.; Retailleau, P.; Iorga, B. I.; Naas, T. (2018) Genetic and Biochemical Characterization of OXA-535, a Distantly-Related OXA-48-like β-Lactamase. *Antimicrob. Agents Chemother.*, AAC.01198-18 DOI 10.1128/AAC.01198-18.

(33) Thomas, V. L.; McReynolds, A. C.; Shoichet, B. K. (2010) Structural Bases for Stability–Function Tradeoffs in Antibiotic Resistance. *J. Mol. Biol.*, *396* (1), 47–59 DOI 10.1016/j.jmb.2009.11.005.

(34) Stojanoski, V.; Chow, D.-C.; Fryszczyn, B.; Hu, L.; Nordmann, P.; Poirel, L.; Sankaran, B.; Prasad, B. V. V.; Palzkill, T. (2015) Structural Basis for Different Substrate Profiles of Two Closely Related Class D β-Lactamases and Their Inhibition by Halogens. *Biochemistry*, *54* (21), 3370–3380 DOI 10.1021/acs.biochem.5b00298.

(35) Dabos, L.; Bogaerts, P.; Bonnin, R. A.; Zavala, A.; Sacré, P.; Iorga, B. I.; Huang, D. T.; Glupczynski, Y.; Naas, T. (2018) Genetic and Biochemical Characterization of OXA-519, a Novel OXA-48-Like β-Lactamase. *Antimicrob. Agents Chemother.*, *62* (8), e00469-18 DOI 10.1128/AAC.00469-18.

(36) Bradford, M. M. (1976) A Rapid and Sensitive Method for the Quantitation of Microgram Quantities of Protein Utilizing the Principle of Protein-Dye Binding. *Anal. Biochem.*, *72*, 248–254.

(37) Naas, T.; Sougakoff, W.; Casetta, A.; Nordmann, P. (1998) Molecular Characterization of OXA-20, a Novel Class D β-Lactamase, and Its Integron from Pseudomonas Aeruginosa. *Antimicrob. Agents Chemother.*, *42* (8), 2074–2083.

(38) Kabsch, W. (2010) Integration, Scaling, Space-Group Assignment and Post-Refinement. *Acta Crystallogr. D. Biol. Crystallogr.*, *66* (Pt 2), 133–144 DOI 10.1107/S0907444909047374.

(39) Legrand, P. (2017) XDSME: XDS Made Easier. *GitHub Repos.*, DOI 10.5281/zenodo.837885.

(40) Evans, P. R.; Murshudov, G. N. (2013) How Good Are My Data and What Is the Resolution? *Acta Crystallogr. D. Biol. Crystallogr.*, *69* (Pt 7), 1204–1214 DOI 10.1107/S0907444913000061.

(41) Winn, M. D.; Ballard, C. C.; Cowtan, K. D.; Dodson, E. J.; Emsley, P.; Evans, P. R.; Keegan, R. M.; Krissinel, E. B.; Leslie, A. G. W.; McCoy, A.; et al. (2011) Overview of the CCP4 Suite and Current Developments. *Acta Crystallogr. D. Biol. Crystallogr.*, *67* (4), 235–242 DOI 10.1107/S0907444910045749.

(42) Keegan, R. M.; Winn, M. D.; IUCr. (2007) Automated Search-Model Discovery and Preparation for Structure Solution by Molecular Replacement. *Acta Crystallogr. Sect. D Biol. Crystallogr.*, *63* (4), 447–457 DOI 10.1107/S0907444907002661.

(43) Emsley, P.; Lohkamp, B.; Scott, W. G.; Cowtan, K. (2010) Features and Development of *Coot*. *Acta Crystallogr. Sect. D Biol. Crystallogr.*, *66* (4), 486–501 DOI 10.1107/S0907444910007493.

(44) Bricogne, G.; Blanc, E.; Brandl, M.; Flensburg, C.; Keller, P.; Paciorek, W.; Roversi, P.; Sharff, A.; Smart, O. S.; Vonrhein, C.; Womack, T. (2011) AutoBUSTER, Version 1.6. 0. *Glob. Phasing Ltd, Cambridge, UK.*,.

(45) Murshudov, G. N.; Skubák, P.; Lebedev, A. A.; Pannu, N. S.; Steiner, R. A.; Nicholls, R. A.; Winn, M. D.; Long, F.; Vagin, A. A. (2011) *REFMAC* 5 for the Refinement of Macromolecular Crystal Structures. *Acta Crystallogr. Sect. D Biol. Crystallogr.*, *67* (4), 355–367 DOI 10.1107/S0907444911001314.

(46) Chen, V. B.; Arendall, W. B.; Headd, J. J.; Keedy, D. A.; Immormino, R. M.; Kapral, G. J.; Murray, L. W.; Richardson, J. S.; Richardson, D. C. (2010) *MolProbity* : All-Atom Structure Validation for Macromolecular Crystallography. *Acta Crystallogr. Sect. D Biol. Crystallogr.*, *66* (1), 12–21 DOI 10.1107/S0907444909042073.

(47) Pettersen, E. F.; Goddard, T. D.; Huang, C. C.; Couch, G. S.; Greenblatt, D. M.; Meng, E. C.; Ferrin, T. E. (2004) UCSF Chimera - A Visualization System for Exploratory Research and Analysis. *J. Comput. Chem.*, *25* (13), 1605–1612 DOI 10.1002/jcc.20084.

(48) Pronk, S.; Páll, S.; Schulz, R.; Larsson, P.; Bjelkmar, P.; Apostolov, R.; Shirts, M. R.; Smith, J. C.; Kasson, P. M.; van der Spoel, D.; Hess, B.,

Lindahl, E. (2013) GROMACS 4.5: A High-Throughput and Highly Parallel Open Source Molecular Simulation Toolkit. *Bioinformatics*, *29* (7), 845–854 DOI 10.1093/bioinformatics/btt055.

(49) Kaminski, G. A.; Friesner, R. A.; Tirado-Rives, J.; Jorgensen, W. L. (2001) Evaluation and Reparametrization of the OPLS-AA Force Field for Proteins via Comparison with Accurate Quantum Chemical Calculations on Peptides. *J. Phys. Chem. B*, *105* (28), 6474–6487 DOI 10.1021/JP003919D.

(50) Parrinello, M.; Rahman, A. (1981) Polymorphic Transitions in Single Crystals: A New Molecular Dynamics Method. *J. Appl. Phys.*, *52* (12), 7182–7190 DOI 10.1063/1.328693.

(51) Hoover, W. G. (1985) Canonical Dynamics: Equilibrium Phase-Space Distributions. *Phys. Rev. A*, *31* (3), 1695–1697 DOI 10.1103/PhysRevA.31.1695.

(52) Nosé, S. (1984) A Unified Formulation of the Constant Temperature Molecular Dynamics Methods. *J. Chem. Phys.*, *81* (1), 511–519 DOI 10.1063/1.447334.

(53) Essmann, U.; Perera, L.; Berkowitz, M. L.; Darden, T.; Lee, H.; Pedersen, L. G. (1995) A Smooth Particle Mesh Ewald Method. *J. Chem. Phys.*, *103* (19), 8577–8593 DOI 10.1063/1.470117.

(54) Hess, B. (2007) P-LINCS: A Parallel Linear Constraint Solver for Molecular Simulation. *J. Chem. Theory Comput.*, *4* (1), 116–122 DOI 10.1021/ct700200b.

.

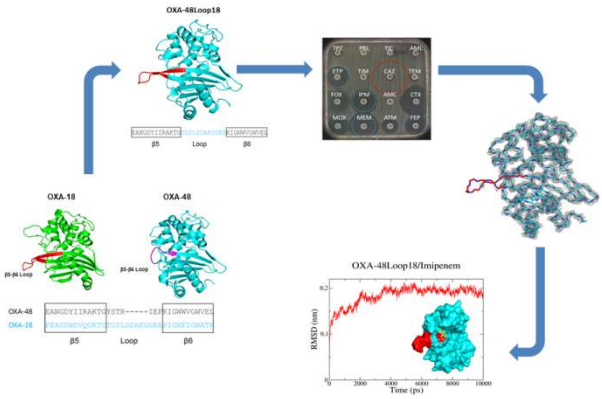
OXA-48Loop18
β5
Loop
β6
OXA-18
OXA-48
β5
Loop
β6
OXA-48Loop18/Imipenem
RMSD (nm)
Time (ps)

Supporting information

Substrate specificity of OXA-48 after β5-β6 loop replacement.

Laura Dabos[‡§#], Agustin Zavala[‖#], Rémy A. Bonnin[‡§⊥], Oliver Beckstein[†], Pascal Retailleau[‖], Bogdan I. Iorga[‖*], Thierry Naas[‡§⊥⊤*]

‡ EA7361 "Structure, dynamic, function and expression of broad spectrum β-lactamases", Université Paris Sud, Université Paris Saclay, LabEx Lermit, Faculty of Medicine, 94270 Le Kremlin-Bicêtre, France.

§ Evolution and Ecology of Resistance to Antibiotics Unit, Institut Pasteur – APHP -Université Paris Sud, 75015 Paris, France

‖ Institut de Chimie des Substances Naturelles, CNRS UPR 2301, Université Paris-Saclay, Labex LERMIT, 91190 Gif-sur-Yvette, France.

⊥ Associated French National Reference Center for Antibiotic Resistance: Carbapenemase-producing Enterobacteriaceae, 94270 Le Kremlin-Bicêtre, France.

† Department of Physics and Center for Biological Physics, Arizona State University, Tempe, 85281 Arizona, USA.

⊤ Bacteriology-Hygiene unit, Assistance Publique/Hôpitaux de Paris, Bicêtre Hospital, 94270 Le Kremlin-Bicêtre, France.

Corresponding Authors

* Thierry Naas, thierry.naas@aphp.fr, and Bogdan I. Iorga, bogdan.iorga@cnrs.fr.

This PDF file includes:

Figures S1 to S4

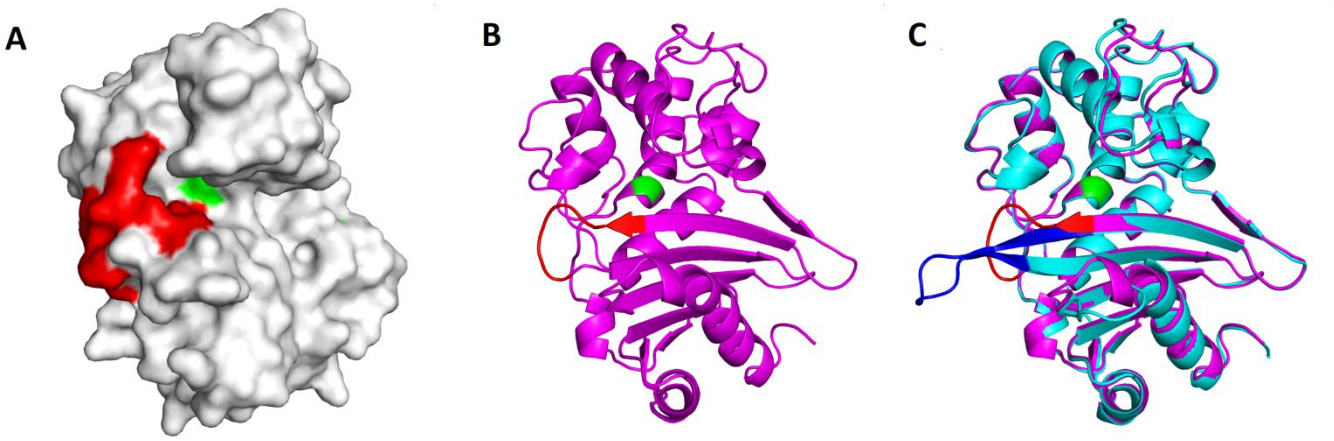

Figure S1. Structure of OXA-48 and β5-β6 loop replacement. Active site serine 70 is colored green and observed at the bottom of the active site cavity, for reference. A) Surface representation of OXA-48, showing the active site cavity wall formed by the β5-β6 loop, depicted in red. B) Backbone representation of OXA-48 showing the orientation of its β5-β6 loop. C) Backbone representation of OXA-48loop18 (cyan) superposed on OXA-48 (magenta), showing the difference in conformation of the replaced β5-β6 loop (red and blue for OXA-48 and OXA-48loop18, respectively).

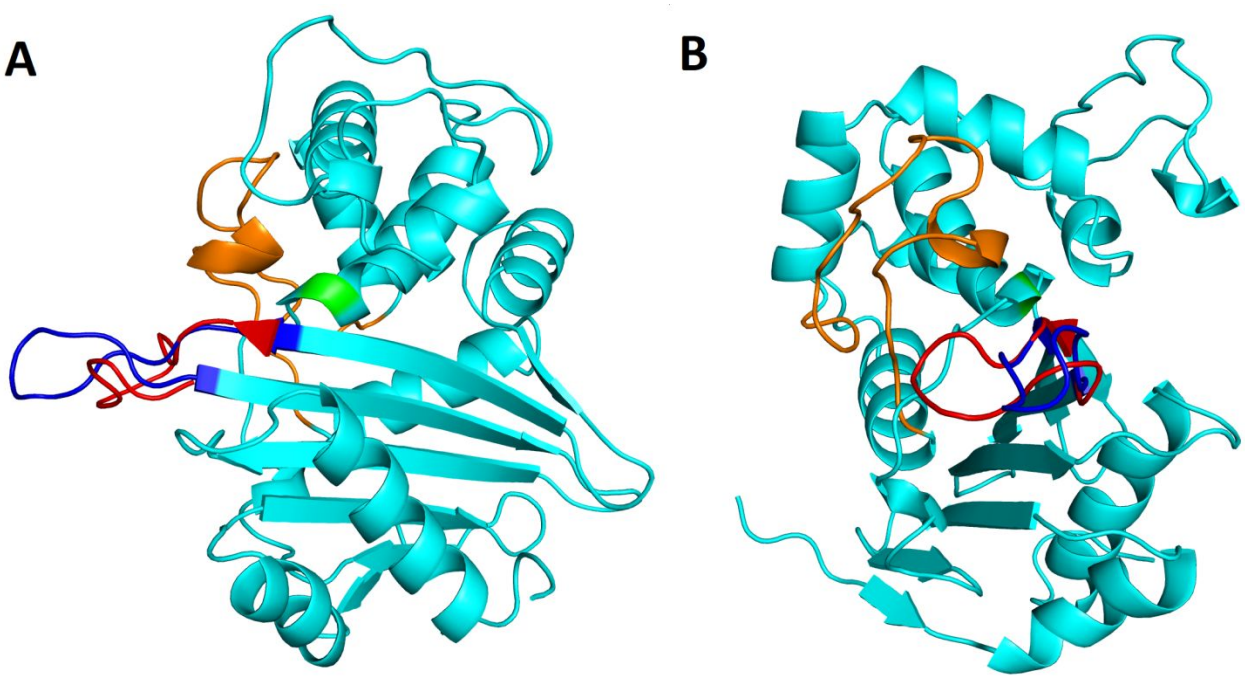

Figure S2. Conformation of β5-β6 loop in OXA-48Loop18 crystal structure. Front view (A) and side view (B). Backbone representation of OXA-48loop18, colored cyan. For reference, active site serine 70 and Ω loop, at the left of the active site, are colored green and orange, respectively. Chains A and B in the crystal structure of OXA-48Loop18 show their β5-β6 loops in a different orientation, with this loop extending away from the active site cavity in chain B (colored blue) and folding back towards the Ω loop in chain A (colored red).

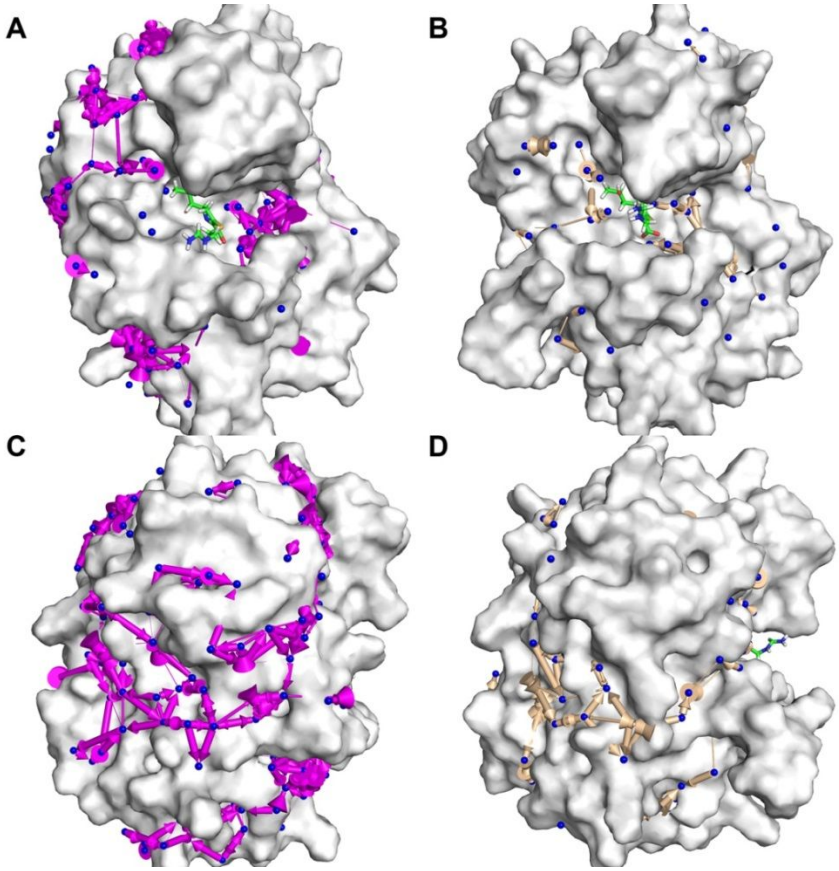

Figure S3. Water networks around OXA-48 and OXA-48Loop18 complexes with imipenem. Dynamic water networks around the protein surface, determined by HOP analysis. It shows the position where water molecules would interact with the protein surface, and how they are proposed to "jump" between positions. A) OXA-48/imipenem complex, front view. B) OXA-48Loop18/imipenem complex, front view. C) OXA-48/imipenem complex, back view. D) OXA-48Loop18/imipenem complex, back view. Notice the larger amount of conserved water sites obtained for OXA-48/imipenem simulations relative to OXA-48Loop18/imipenem.

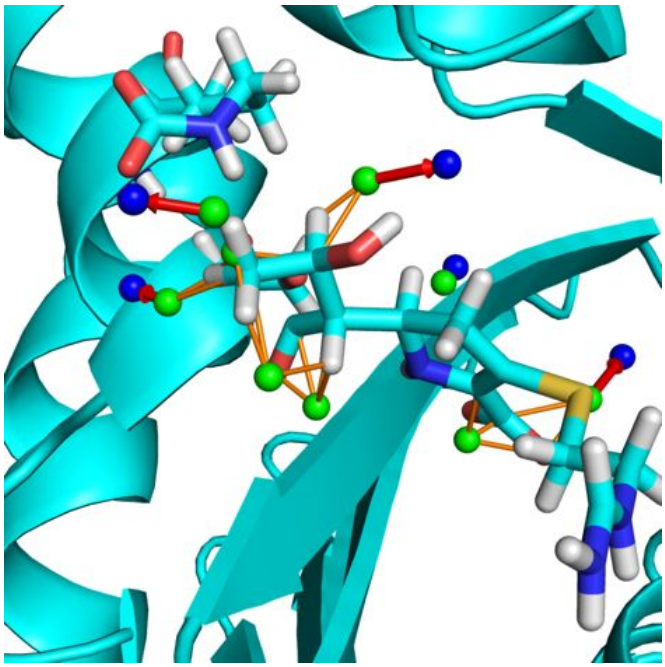

Figure S4. Displacement of active site water molecules by imipenem. Conserved water molecule sites determined by HOP for simulations of OXA-48 (green spheres) and OXA-48-imipenem covalent complex (blue spheres). Overlaps displayed with orange lines. Notice the shift (red arrows) of certain water molecule sites caused by the presence of imipenem in the active site. Other water molecule binding positions are simply filled by the antibiotic, such as the oxyanion hole or the pocket for the C3 carboxylate.